Mineralium Deposita (2003) 38: 739–750
DOI 10.1007/s00126-003-0368-x

ARTICLE

Hong Rui Fan · Ming Guo Zhai · Yi Han Xie
Jin Hui Yang

Ore-forming fluids associated with granite-hosted gold mineralization at the Sanshandao deposit, Jiaodong gold province, China

Received: 8 November 2001 / Accepted: 9 May 2003 / Published online: 28 June 2003

Abstract The Sanshandao gold deposit, with total resources of more than 60 t of gold, is located in the Jiaodong gold province, the most important gold province of China. The deposit is a typical highly fractured and altered, disseminated gold system, with high-grade, quartz-sulphide vein/veinlet stockworks that cut Mesozoic granodiorite. There are four stages of veins that developed in the following sequence: (1) quartz-K-feldspar-sericite; (2) quartz-pyrite ± arsenopyrite; (3) quartz-base metal sulfide; and (4) quartz-carbonate. Fluid inclusions in quartz and calcite in vein/veinlet stockworks contain C-O-H fluids of three main types. The first type consists of dilute CO_2–H_2O fluids coeval with the early vein stage. Molar volumes of these CO_2–H_2O fluid inclusions, ranging from 50–60 cm^3/mol, yield estimated minimum trapping pressures of ≥3 kbar. Homogenization temperatures, obtained mainly from CO_2–H_2O inclusions with lower CO_2 concentration, range from 267–375 °C. The second inclusion type, with a CO_2–$H_2O \pm CH_4$ composition, was trapped during the main mineralizing stages. These fluids may reflect the CO_2–H_2O fluids that were modified by fluid/rock reactions with altered wallrocks. Isochores for CO_2-$H_2O \pm CH_4$ inclusions, with homogenization temperatures ranging from 204–325 °C and molar volumes from 55 to 70 cm^3/mol, provide an estimated minimum trapping pressure of 1.2 kbar. The third inclusion type, aqueous inclusions, trapped in cross-cutting microfractures in quartz and randomly in calcite, are post-mineralization, and have homogenization temperatures between 143–228 °C and salinities from 0.71–7.86 wt% NaCl equiv. Stable isotope data show that the metamorphic fluid contribution is minimal and that ore fluids are of magmatic origin, most likely sourced from 120–126 Ma mafic to intermediate dikes. This is consistent with the carbonic nature of the fluid, and the cross-cutting nature of those deposits relative to the host Mesozoic granitoid.

Keywords Fluid inclusion · Orogenic gold deposit · Sanshandao · Jiaodong

Editorial handling: R.J. Goldfarb

H. R. Fan (✉) · M. G. Zhai · Y. H. Xie · J. H. Yang
Key Laboratory of Mineral Resources,
Institute of Geology and Geophysics,
Chinese Academy of Sciences, P.O. Box 9825,
100029 Beijing, China
E-mail: fanhr@mail.igcas.ac.cn
Tel.: +86-10-62008088
Fax: +86-10-62010846

Introduction

The Jiaodong gold province is located on the Jiaodong Peninsula of eastern China (Fig. 1). It is currently the most important gold producer in China, both in terms of gold production (55 t in 2000), and gold ore reserves that are >900 t (China National Gold Bureau, unpublished data). Several world-class (>100 t) gold districts have been discovered on the Jiaodong Peninsula during the past two decades. More than 80% of the gold reserves are concentrated in the Zhaoyuan-Laizhou (or Zhao-Ye) gold belt (Fig. 1) within an area of about 3,500 km^2.

The Jiaodong gold province occurs along the southeastern margin of the North China craton, which is dominated by Archaean rock units. It is bounded by the N- to NE-trending Tan-Lu fault zone to the west and by the Su-Lu ultrahigh pressure metamorphic belt to the south (Fig. 1). Supracrustal rocks in the northwestern part of the Jiaodong Peninsula comprise both metamorphosed Precambrian sequences and Mesozoic volcanic rocks and intrusions (Wang et al. 1998; Zhou and Lu 2000). The Precambrian sequence is composed of basement rocks of the Late Archaean Jiaodong Group, which consists of mafic to felsic volcanic and sedimentary rocks metamorphosed to amphibolite to granulite facies. It was determined to be as old as 2,665 ± 9 Ma by conventional U-Pb zircon methods (Qiu 1989). Plutonic

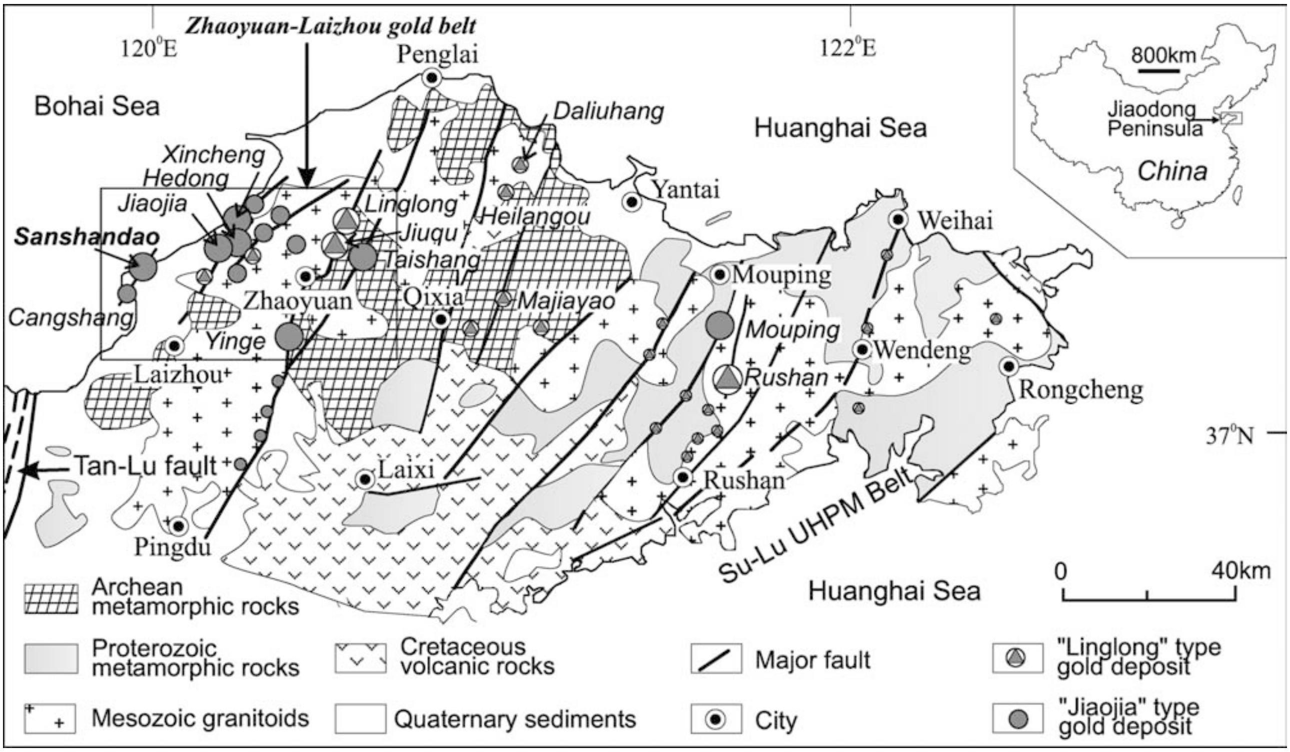

Fig. 1 Simplified geological map of the Jiaodong Peninsula showing location of the major gold deposits (after Yang 2000). Differently sized symbols of gold deposits mean different gold resources, *big symbol* means Au≥50 t, *small symbol* means Au < 50 t. The Sanshandao deposit occurs along the western margin of the gold province

rocks, which intruded into the Precambrian basement in the northwestern part of the Jiaodong Peninsula, have been traditionally divided into two suites, the Linglong and the Guojialing. The Linglong suite consists of medium-grained metaluminous to slightly peraluminous biotite granite, and the Guojialing suite is composed of porphyritic hornblende-biotite granodiorite. The ages of emplacement of these granitoid suites are 160–156 Ma and 130–126 Ma (SHRIMP U-Pb zircon data; Wang et al. 1998; Qiu et al. 2002), respectively.

The major gold deposits of the Jiaodong Peninsula are hosted in Mesozoic granitoids. Two main phases of deformation occurred in this district during the Mesozoic; the first phase, northwest-southeast oblique compression, produced prominent NNE- to NE-trending brittle-ductile shear zones with sinistral oblique reverse movements, and the second phase involved the development of brittle structures, accompanied by hydrothermal alteration and gold mineralization (Wang et al. 1998; Hu et al. 1998; Zhai et al. 2002). Most of the gold deposits comprise a quartz-K-feldspar, quartz-pyrite, quartz-base metal sulfide, and quartz-carbonate paragenetic sequence (Chen et al. 1989; Lu and Kong 1993; Wei and Qiu 1993; Zhai et al. 2001; Qiu et al. 2002). The numerous mafic to intermediate dikes that were emplaced simultaneously with formation of the gold lodes are dated at 124–120 Ma (K-Ar whole rock isochron ages, Yang 2000). Recent direct Rb-Sr dating of pyrite from the major Linglong gold deposit in the Jiaodong district shows gold mineralization occurred at about 123–122 Ma (Yang and Zhou 2001). Zhang et al. (2003) dated sericite at 121.3 ± 0.2 Ma by ^{40}Ar-^{39}Ar methods in the Cangshang gold deposit which is located in the same fault zone as the Sanshandao deposit (Fig. 1).

Gold deposits of the Jiaodong Peninsula are divided into two types, "Linglong-type" and "Jiaojia-type" (Fig. 1). Linglong-type quartz vein-style gold mineralization, typically hosted in second- or third-order faults cutting Mesozoic granitoids, occurs as single or multiple, relatively continuous quartz veins. Disseminated- and stockwork-style Jiaojia-type gold mineralization occurs along first-order regional faults, which are surrounded by broad alteration halos. The variation in style of the deposits appears to result from the degree of deformation within the host structures, and is probably also related to the orientation of the resultant host structures to the regional stress field (Qiu et al. 2002).

Previous fluid inclusion studies of deposits in the province were mostly published in Chinese and mainly focused on the typical Linglong-type deposits (e.g., Xu et al. 1996; Lu et al. 1999), with less common and more recent studies on Jiaojia-type ores. Shen et al. (2000) carried out a preliminary fluid inclusion study of the Jiaojia-type Yinge deposit along the Zhaoyuan-Pingdu fault zone. They observed two-phase aqueous inclusions and CO_2–H_2O two- or three-phase inclusions with variable liquid-vapour ratios. Mineralizing temperatures were estimated to be 180–275 °C with fluid pressures of about 1.5 kbar. Lu et al. (1999) examined Linglong-type vein deposits in the Linglong district. Fluids in these veins were found to have a CO_2-H_2O-NaCl composition with a salinity of 4–9 wt% NaCl eq. Homogenization temperatures varied from 100–380 °C.

The Sanshandao Jiaojia-type gold deposit, first discovered in 1967 and originally developed by local prospectors for the first few years, is now being worked by the Sanshandao Gold Company, with an estimated annual production of > 1 t. About 5 km south of Sanshandao, along the same fault zone, the 2 Moz Au Jiaojia-type Cangshang deposit is located (Zhang et al. 2003). As the Jiaojia-type deposits are now recognized as the most important gold resources in the province (e.g., Jiaojia and Xincheng deposits also each with 2 Moz Au), research on the ore-forming fluids at the Sanshandao deposit has broad metallogenic and exploration implications. Our study builds on existing geological, petrographic and geochemical information about the Sanshandao deposit (Chen et al. 1989; Yang and Lu 1996; Yang et al. 1998).

Geological setting

The Sanshandao gold deposit is located in the western part of the Jiaodong gold province, about 30 km north of Laizhou City (Fig. 1). The gold mineralization is confined to a major fault zone (Sanshandao fault) that cuts the Sanshandao granodiorite (Fig. 2), a body of the Guojialing granodiorite suite. The deposit is a typical Jiaojia-type gold system with a high density of high-grade, quartz-sulphide veinlets and stockworks. The bulk of the ore is disseminated within the altered granite, characterized by strong silicification, sericitization, sulphidation and K-feldspar alteration (Qiu et al. 2002). The Sanshandao granodiorite occurs as a small NE-SW-trending stock emplaced into the mafic and intermediate gneisses, and migmatized amphibolites of the Archaean Jiaodong Group (Fig. 2). Mineral phases of the pluton consist of 18–24% K-feldspar, 47–53% plagioclase, 18–22% quartz, 3–8% biotite, and 2–5% amphibole (Chen et al. 1989).

Two styles of Jiaojia-type gold mineralization can be distinguished at the Sanshandao deposit. The most common style comprises disseminated gold within sericite-, quartz- and pyrite-altered granodiorite along the Sanshandao fault. Lesser amounts of K-feldspar, carbonate and, locally, chlorite are also present. The other style comprises gold-quartz vein/veinlet stockworks mainly within the altered granitoid and, less commonly, in the Archaean gneiss. Samples collected for fluid inclusion and isotope studies were mainly from the stockworks. Gold-bearing zones are mainly controlled by the NE-SW-trending Sanshandao fault. Structures along the fault zone are characterized by early shearing and late brittle fracturing, throughout a zone > 5 km long and 200 m in width. The ore-bearing zones trend northeast (20–40°), dip (35–70°) southeast, and extend offshore into the Bohai Sea (Fig. 1). Six orebodies have been found at the Sanshandao deposit. The largest ore body, No.1, is 1,020 m long, averages 0.4 to 6.2 m in thickness, and continues to approximately 900 m in depth. The major orebodies are concentrated in dilational zones within shear zones and faults along the main fault. Gold grades range from 3 to 10 g/t, with total resources in the six orebodies of more than 60 t.

Ore-bearing veins and their mineral assemblages

The main hydrothermal minerals associated with gold mineralization include pyrite, galena, sericite and K-feldspar, with lesser arsenopyrite, sphalerite, chalcopyrite, chlorite, and siderite. Studies of mineral paragenesis and ore structures distinguish four stages of mineralization for ore-bearing lode systems (Chen et al. 1989):

Stage 1, quartz-K-feldspar-sericite

This stage is located in an outer reddish alteration zone, which extends for as much as several hundred meters, and is defined by small-scale, milky white quartz veins/veinlets or pods, with K-feldspar and variable amounts of sericite in the surrounding alteration zones. Minor coarse euhedral and subhedral pyrite occurs. Gold is not deposited in this stage.

Fig. 2 **a** General geological map and **b** cross section of the Sanshandao gold deposit (after Chen et al. 1989). Gold-bearing zones at the Sanshandao deposit are mainly controlled by the NE-SW-trending Sanshandao fault which cuts the Sanshandao granodiorite

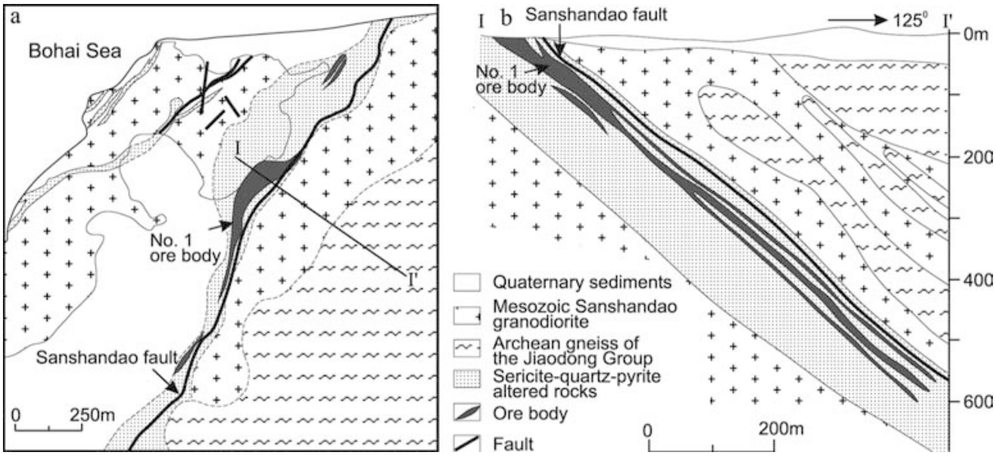

Stage 2, quartz-pyrite ± arsenopyrite

This stage consists of white-grey quartz vein networks containing pyrite, with minor arsenopyrite and chalcopyrite. Pyrite occurs as coarse euhedral cubes and subhedral aggregates, and arsenopyrite as fine-grained subhedral and anhedral aggregates. Fine-grained gold occurs in quartz or sulfide minerals, particularly in pyrite.

Stage 3, quartz-base metal sulfide

This stage is characterized by precipitation of large amounts of sulfide minerals (pyrite, arsenopyrite, galena, sphalerite, and chalcopyrite) and constitutes the major gold mineralization period. Quartz is dark-grey in colour and pyrite occurs as fine-grained subhedral and anhedral aggregates. The other sulfide minerals occur as fine-grained anhedral aggregates, typically filling microcracks in pyrite and quartz. Gold mainly fills cracks within pyrite and arsenopyrite, and less commonly within sphalerite and galena (Chen et al. 1989).

Stage 4, quartz-carbonate

This stage is composed mainly of quartz, calcite and siderite, with very minor pyrite. In some cases, veins and veinlets of only calcite or siderite occur. Gold mineralization is very low grade in this stage.

In summary, the gold mineralization at the Sanshandao deposit is mainly concentrated in paragenetic stages 2 and 3. Gold occurs as native gold and as electrum in pyrite, with minor free gold and electrum in the quartz and also altered wallrocks. Typical native gold contains 10–20 wt% Ag, and electrum contains 68–78 wt% Au.

Fluid inclusion petrography

Fluid inclusions were examined in 30 samples from all four paragenetic stages. There were abundant fluid inclusions in quartz grains of stages 1 to 3, and less suitable fluid inclusions were found in quartz and carbonate of stage 4 veins. Measurements were carried out on 21 doubly polished sections (about 200–300 μm thick). Three compositional types of fluid inclusions were identified based on their optical characteristics at room temperature, using the criteria of Roedder (1984) and phase transitions during microthermometric measurements (Diamond 2001).

CO_2–H_2O fluid inclusions

CO_2-H_2O inclusions have negative crystal shapes and occur in quartz of stages 1 and 2. These inclusions generally consist of two phases (Fig. 3a), an aqueous phase and a liquid CO_2 bubble, at room temperature, showing a V_{CO2} of 0.3–0.7 (visual estimation at 25 °C). The inclusions generally range in diameter from less than 15 μm to rarely as much as 30 μm. These inclusions are interpreted to contain the fluid that deposited early quartz of stage 1.

CO_2–$H_2O \pm CH_4$ fluid inclusions

Inclusions containing CO_2–$H_2O \pm CH_4$ occur as isolated cavities or planar arrays in healed microfractures in vein

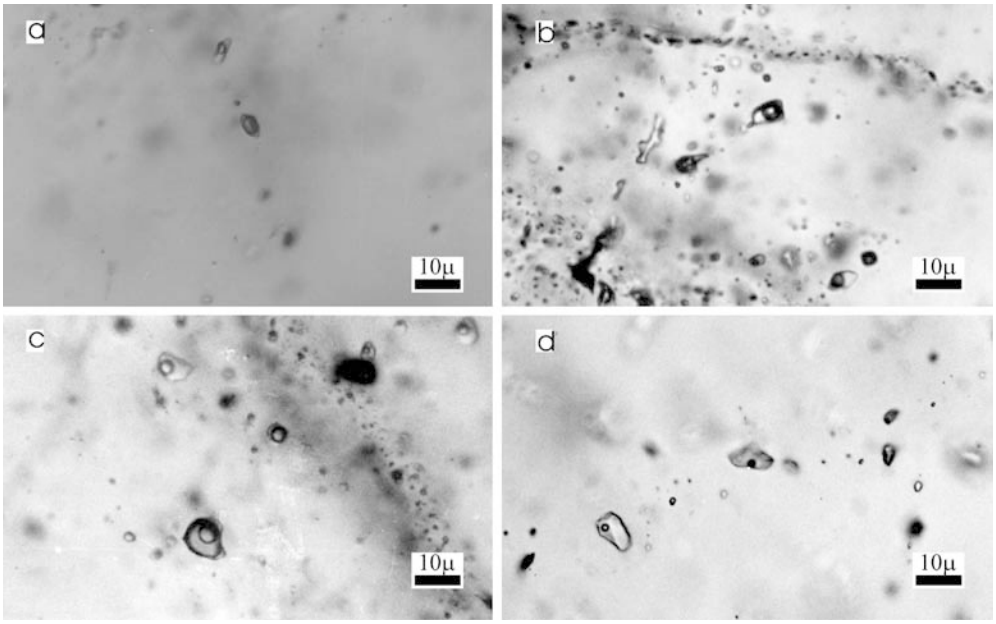

Fig. 3 Photomicrographs showing: **a** CO_2–H_2O fluid inclusions in quartz-K-feldspar–sericite vein. **b** Three-phase CO_2–$H_2O \pm CH_4$ inclusions in quartz-pyrite ± arsenopyrite vein. **c** Two- and three-phase CO_2–$H_2O \pm CH_4$ inclusions with varying phase ratios in quartz–sulfide vein. **d** Secondary aqueous fluid inclusions within quartz-sulfide vein. All inclusions are in quartz

quartz from stages 2 and 3. The inclusions are generally less than 20 µm in diameter and occur as: (1) three phases consisting of an aqueous liquid, a carbonic liquid and vapor with relatively constant phase ratios (Fig. 3b), or (2) two- or three-phases consisting of an aqueous liquid, a carbonic liquid and/or a vapor with varying phase ratios of between 10 and 90% carbonic species (Fig. 3c). Although direct physical contact of fluid inclusions with gold grains was not observed, gold grains are intergrown with sulfide minerals and/or quartz in stage 2 and 3 assemblages; thus, these fluid inclusions are thought to represent the gold-bearing fluids.

Aqueous fluid inclusions

Aqueous inclusions consist of an aqueous liquid and a small vapor phase and appear with a filling degree of 85–95 vol% liquid. The inclusions occur as secondary trails in microfractures cutting quartz grains (Fig. 3d) of all stages or as random inclusions in calcite in stage 4 veins. They reach 15 µm in maximum dimension. These inclusions are interpreted to contain a fluid trapped late in the hydrothermal history of the system.

Microthermometric results

The microthermometric study of fluid inclusions was carried out with a Leitz microscope and a Linkam THMS 600 programmable heating-freezing stage (Shepherd et al. 1985) at the Institute of Geology and Geophysics, Chinese Academy of Sciences (IGGCAS). Most measurements were made at a heating rate of 0.2 to 0.4 °C/min. Carbonic phase melting ($TmCO_2$) and clathrate melting (Tmclath) were determined by temperature cycling (Roedder 1984; Diamond 2001); the heating rate near $TmCO_2$ and Tmclath was 0.1–0.2 °C/min for measurements. Accuracy of the measurements was ensured by calibration against the triple-point of pure CO_2 (−56.6 °C), the freezing point of water (0.0 °C) and the critical point of water (374.1 °C) using synthetic fluid inclusions supplied by FLUID INC. The reproducibility of measurements was ±0.2 °C below +30 °C and ±2°C at temperatures of final homogenization, where the chips were centered in the specimen holder. In order to confirm the suggested fluid inclusion volatile species, representative samples were analyzed using a Renishaw 1000 Raman microspectrometer at IGGCAS according to the method of Burke (2001).

The microthermometric data from all types of fluid inclusions are summarized in Table 1 and graphically presented for all measurements of the two generations of CO_2-bearing inclusions in Fig. 4. Calculations of salinity, mole fractions of compositions (X_{H2O}, X_{CO2}, X_{NaCl}), density of carbonic liquid and bulk fluid, and bulk molar volume of fluid inclusions were made using the MacFlincor computer software (Brown and Hagemann 1995) and a computer program to calculate salinity from clathrate melting temperature (Bakker 1997). The molar volume and X_{CH4} of the carbonic phase was calculated from the homogenization temperature of the carbonic phase ($ThCO_2$) and melting temperature of the carbonic phase ($TmCO_2$) using the method of Thiéry et al. (1994).

Pre-gold CO_2–H_2O fluid inclusions

The CO_2–H_2O fluid inclusions freeze to a solid phase below −95 °C. During heating runs, melting of the carbonic phase ($TmCO_2$) occurs either at the CO_2 triple point of −56.6 °C, or over a small interval with depressed melting temperatures between −57.5 and −56.7 °C (Table 1, Fig. 4a). These measurements indicate that the carbonic phase in these inclusions is nearly pure CO_2, in contrast to gold-related inclusions with depressed melting temperatures (e.g., see below discussion of CO_2–$H_2O \pm CH_4$ fluid inclusions) that probably contain minor amounts of additional gas species, most likely CH_4 and/or N_2 (Burruss 1981).

Melting of the CO_2 clathrate (Tmclath) in the presence of CO_2 liquid occurs between 5.4 and 10.2 °C (Fig. 4a), below and just above the invariant point of a pure CO_2 clathrate (10 °C; Hollister and Burruss 1976). Partial homogenization ($ThCO_2$) of CO_2 liquid + CO_2 vapor to liquid CO_2, less commonly to vapor, occurs between 7.4 and 22.4 °C (Fig. 4a). As Raman peaks were not detected for N_2 and H_2S in these inclusions, these species are assumed to be very minor. The calculated X_{CH4} in the carbonic phase using the method of Thiéry et al. (1994) and MacFlincor software (Brown and Hagemann 1995) is generally less than 0.05, and X_{CO2} varies from 0.13 to 0.57. The CO_2 densities of the carbonic phase are 0.81–0.94 g/cm^3, and densities of the bulk inclusions range from 0.83 to 0.97 g/cm^3. Calculated salinities of the aqueous phase in these inclusions are ≤ 8.4 wt% NaCl equiv, with most ranging from 4.1–8.1 wt% NaCl equiv. Upon heating runs, more than one-half of the studied inclusions decrepitated prior to final homogenization, at temperatures from 215–320 °C. Total homogenization temperatures to liquid, obtained mainly from inclusions with lower CO_2 contents and smaller diameters, range from 267–375 °C (Table 1).

CO_2–$H_2O \pm CH_4$ fluid inclusions

The $TmCO_2$ during heating runs of the CO_2-$H_2O \pm CH_4$ inclusions takes place from −65.6 to −56.8 °C (Fig. 4b), and is thus suggestive of significant amounts of other non-aqueous phases, in addition to CO_2, in many inclusions. The Tmclath measurements were between 6.4 and 13.5 °C for these same inclusions (Fig. 4b). The presence of CH_4 was verified with laser Raman microspectrometry for two samples. Partial homogenization of CO_2-CH_4 liquid and CO_2-CH_4 vapor, consistently to a liquid, occurs over a wide range from −8.3–26.8 °C (Fig. 4b). The inclusions

Table 1 Fluid inclusion data (in °C) from the Sanshandao gold deposit

Sample no.	Host mineral[a] inclusion type[b]	$TmCO_2$	Tmclath[c]	$ThCO_2$(l) ($ThCH_4$ = *)	Th(tot)[d]
Ss-1–2	qz/1	−56.9 to −57.5	9.8 (hydr)	12.4 to 18.8	282 to 355 (l)
Ss-1–3	qz/1	−56.6 to −56.8	5.8 to 7.1 (hydr)	7.4 to 15.6	271 to 332 (l), 348 (g)
	qz/2	−57.0 to −57.9	8.3 to 10.5 (hydr)	13.2 to 25.8	204 to 285 (l)
Ss-2–1	qz/1	−56.8 to −57.3		9.5 to 15.6	327 to 368 (l)
	qz/3		−1.4 to −3.1 (ice)		143 to 156 (l)
Ss-2–3	qz/2	−58.1 to −60.3		11.2 to 22.1	245 to 293 (l)
	qz/3		−0.8 to −4.0 (ice)		165 to 199 (l)
Ss-2–4	qz/1	−56.8 to −57.0	5.4 to 6.6 (hydr)	12.1 to 18.5	305 (l)
	qz/2	−57.3 to −60.9	6.4 to 10.3 (hydr)	7.1 to 23.4	231 to 284 (l)
Ss-2–7	qz/1	−57.2 to −57.4		14.7 to 20.6	267 to 340 (l), 304 (g)
	qz/2	−59.2	8.9 (hydr)		
Ss-2–9	Cc/3		−2.2 to −5.0 (ice)		150 to 213 (l)
Ss-3–2	qz/2	−64.9	11.3 (hydr)	0.5	318 (g)
Ss-3–4	qz/1	−56.8 to −57.1		16.4 to 19.0	283 to 339 (l), 375 (g)
	qz/2	−57.6 to −58.2	7.1 to 8.6 (hydr)	7.2 to 14.2	213 to 291
Ss-3–5	qz/2	−57.1 to −58.9	7.2 to 10.2 (hydr)	18.2 to 21.5	225 to 282 (l)
	qz/3		−2.1 to −4.2 (ice)		185 (l)
Ss-3–6	cc/3		−1.8 to −3.7 (ice)		163 to 189(l)
Ss-4–1	qz/2	−57.2 to −57.9	7.0 to 10.7 (hydr)	13.4 to 23.8	243 to 286 (l), 278 (c)
Ss-4–4	qz/1	−56.8 to −57.1	7.3 to 9.9 (hydr)	12.4 to 15.6	324 (l)
Ss-4–5	qz/1	−56.7 to −56.9	9.0 to 10.2	15.1 to 18.3	295 (l), 342 (g)
	qz/2	−57.1 to −57.7	6.8 to 10.5 (hydr)	21.1 to 26.8	209 to 275 (l)
	qz/2		15.6 (hydr)	−82.5 to −87.0*	
Ss-5–1	qz/2	−58.3	8.1 (hydr)	15.3	
Ss-5–3	qz/2	−60.3 to −62.8	8.7 to 13.5 (hydr)	−5.9 to 5.0	280 (l)
Ss-5–7	qz/1	−56.9 to −57.5	5.4 to 6.0 (hydr)	13.5 to 16.6	347 (g)
	qz/2	−57.8 to −58.3	7.0 to 10.1 (hydr)	22.3 to 25.5	225 to 295 (l)
Ss-5–8	qz/2	−61.6	13.5 (hydr)	4.6	245 (l)
	qz/3		−2.5 to −4.3 (ice)		157 to 179 (l)
Ss-6–2	qz/1	−57.0	8.9 (hydr)	22.4	315 (l)
Ss-6–3	qz/2	−65.6	12.4 (hydr)	−8.3	
Ss-6–5	qz/1	−56.8 to −56.9		14.8 to 18.9	
	qz/2	−58.6	8.0 (hydr)	15.3	302(l)
	qz/3		−0.4 to −4.2 (ice)		184 to 228(l)

[a] qz, Quartz; cc, calcite

[b] 1, CO_2-H_2O fluid inclusion; 2, CO_2-$H_2O \pm CH_4$fluid inclusion; 3, aqueous fluid inclusion

[c] ice, melting of ice; hydr, dissociation of gas-hydrates

[d] l, homogenization to liquid; g, homogenization to gas; c, critical homogenization

show a range in final homogenization temperatures to liquid from 204–325 °C (Table 1). It is important to note that these data are mainly from inclusions with relatively small CO_2-CH_4 bubbles ($<$ 40 vol%), because almost all the inclusions with greater volumes of the carbonic phase decrepitated prior to homogenization at temperatures between 226 and 273 °C.

The calculated mole proportions of X_{CH4} in carbonic phase are 0.01–0.26. Integration of the Raman peaks, giving relative amounts of CO_2 and CH_4 for the inclusions, suggests similar CH_4 concentrations. Using MacFlincor software (Brown and Hagemann 1995) and the computer programs of Bakker (1997), calculated X_{CO2} and X_{CH4} in the bulk inclusion are 0.04–0.50 and $<$ 0.01–0.14. The calculated densities of the carbonic phase and bulk inclusion are 0.62–0.98 g/cm^3 and 0.82–0.01 g/cm^3, respectively. The Tm data (Table 1) indicate salinities of $\leq$ 7.1 wt% NaCl equiv. if the CO_2–H_2O–NaCl system is used as a reference (Diamond 1992). However, the presence of significant CH_4 in many inclusions results in increased clathrate melting temperatures. Therefore, the true salinities will be higher than those calculated between 0 and 7.1 wt% NaCl equiv. No correlation between final homogenization temperature and hydrate dissociation temperatures exists. In one sample, some inclusions (Ss-4–5, Table 1) homogenized at about −82.5 to −87.0 °C, suggesting a carbonic phase composed of almost pure CH_4 (van den Kerkhof and Thiéry 1994; ver der Kerkhof 2001).

Aqueous fluid inclusions

The aqueous inclusions showed final homogenization to liquid at temperatures between 143 and 228 °C and melting of ice in the range of −0.4 to −5.0 °C (Table 1). The melting temperatures correspond to salinities from 0.7 to 7.9 wt% NaCl equiv. (Bodnar 1993).

Oxygen and hydrogen stable isotopes

The oxygen isotope compositions of quartz from the veins and from altered and unaltered granitoid have been determined. Eight analyses were carried out on vein quartz, and three quartz samples were separated from the

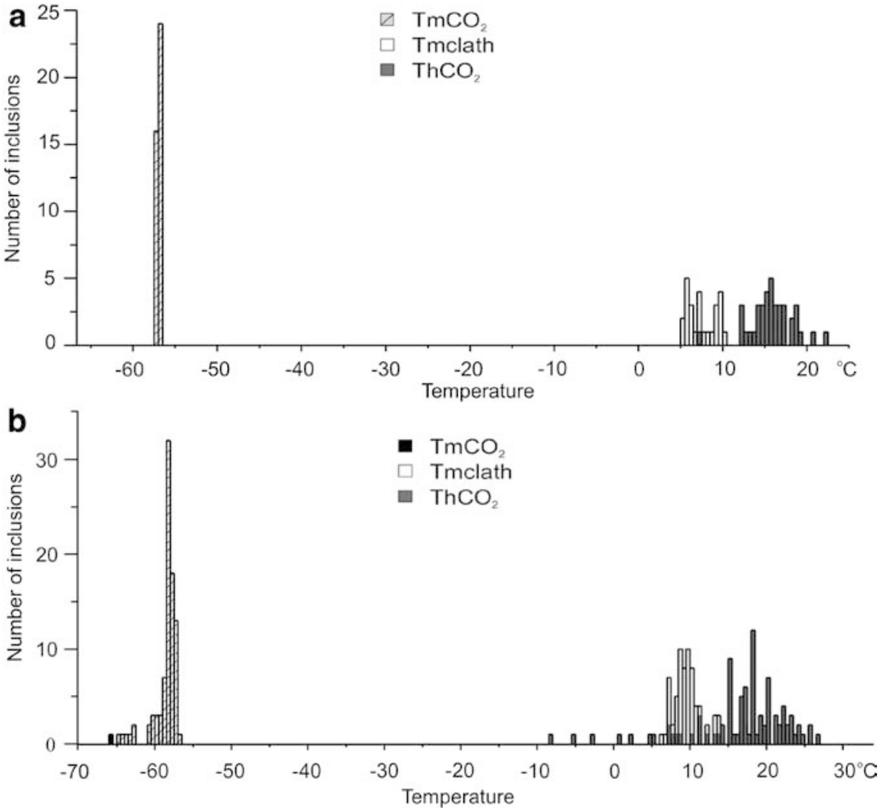

Fig. 4 Histograms of microthermometric measurements from CO_2-bearing fluid inclusions in the Sanshandao deposit. **a** Microthermometric data for $TmCO_2$, Tmclath and $ThCO_2$ of pre-gold, CO_2–H_2O fluid inclusions. **b** Microthermometric data for $TmCO_2$, Tmclath and $ThCO_2$ of gold-related (stages 2 and 3), CO_2–$H_2O \pm CH_4$ fluid inclusions

Table 2 Results from oxygen and hydrogen isotope analyses from the Sanshandao gold deposit

Sample	δ^{18}Oqz (‰)	Th (°C)	T(p correction) (°C)	δ^{18}Ofluid (‰)	δDfluid (‰)	Inclusion
Quartz from stage 1 veins						
Ss-1–2	10.2	325	170	7.8	−63.8	P > > S[a]
Ss-2–1	13.0	340	170	10.9	−67.8	P > S[b]
Ss-6–2	13.4	315	170	10.9	−67.4	P > > S
Quartz from stage 2 and stage 3 veins						
Ss-2–3	13.7	275	80	8.5	−77.2	P > S
Ss-3–5	13.4	250	80	7.5	−79.1	P > S
Ss-4–1	13.2	265	80	7.7	−66.4	P > > S
Ss-5–3	12.8	280	80	7.7	−70.4	P > S
Ss-5–8	13.1	245	80	7.0	−80.6	S > P[c]
Quartz from host rocks (granite)						
Ss-9 (altered granite)	12.5					
Ss-10 (altered granite)	12.2					
Ss-15 (unaltered granite)	10.6					

[a] P >> S, large and abundant primary inclusions-very few and small secondary inclusions
[b] P > S, large and abundant primary inclusions-small and few secondary inclusions
[c] S > P, abundant secondary inclusions-few primary inclusions

host intrusion. The samples were ground to −60, –100 mesh size. Quartz was hand-picked and/or separated using a magnetic separator. Oxygen was liberated from quartz by reaction with BrF_5 (Clayton and Mayeda 1963) and converted to CO_2 on a platinum-coated carbon rod. The δ^{18}O determinations were made on a MAT-252 mass spectrometer. Reproducibility for isotopically homogeneous pure quartz is about ±0.1‰ (1σ).

Analyses of hydrogen isotopic compositions of the inclusion fluids have been made on the eight quartz vein samples. Water was released by heating the samples to approximately 500 °C in an induction furnace. Samples were first degassed of labile volatiles by heating under vacuum to 120 °C for 3 h. Water was converted to hydrogen by passage over heated zinc powder at 410 °C (Friedman 1953) and the hydrogen was analyzed with a MAT-252 mass spectrometer. Analyses of standard water samples suggest a precision for δD of ±3‰ (1σ). All stable isotopic analyses were performed at IGGCAS. Results are presented in Table 2.

Oxygen isotopic compositions of hydrothermal waters in equilibrium with quartz were calculated using an extrapolation of the fractionation formula from Clayton et al. (1972). The calculations of the fractionation factors were made using the mean value of the homogenization temperatures of fluid inclusions from the same quartz samples plus pressure-corrected temperature as discussed below. The calculated oxygen isotope composition of the fluid varies between 7.0and 10.9 ‰ (Table 2). The analyses of hydrogen isotopic composition, measured directly on inclusion fluid, gave a relatively narrow spread between −63.8 and −80.6‰. In a plot of δD vs. $\delta^{18}O$ (Fig. 5) eight quartz samples plot within or just adjacent to the primary magmatic water field.

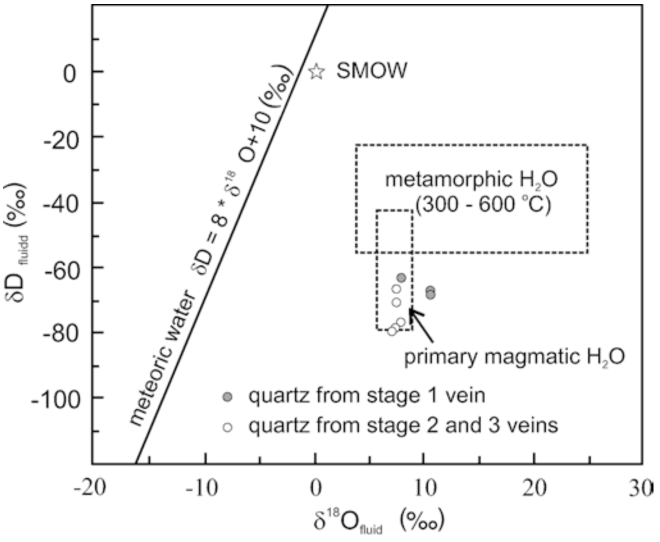

Fig. 5 Fluid δD and $\delta^{18}O$ characteristics of the gold-depositing fluids at Sanshandao. Also shown are the isotopic fields for common geological waters (Taylor 1979)

The oxygen isotopic compositions of quartz from the altered granitoid (Table 2) are also likely to have been affected by the gold-depositing fluids. Using the quartz-H_2O oxygen isotopic fractionation (Matsuhisa et al. 1979) as an approximation for the rock-fluid fractionation, the fluid in equilibrium with the altered granitoid ($\delta^{18}O$-value of quartz up to + 12 ‰) at Sanshandao has a calculated $\delta^{18}O$ composition of ca. + 10‰ at 500 °C, which is isotopically the same as the value of the Au-depositing fluid.

Discussion

Hydrothermal fluid composition

The pre-gold CO_2–H_2O fluid inclusions occur isolated in samples of early white quartz and are assumed to have been trapped during crystallization of the earliest quartz. The molar volumes of these CO_2-H_2O fluid inclusions are 50 ~60 cm^3/mol (Fig. 6). Fluid inclusions associated with Au mineralization contain mostly CO_2-$H_2O \pm CH_4$ inclusions, and occur isolated, and sometimes in healed fractures particularly in stockwork quartz. The molar volumes of the CO_2–$H_2O \pm CH_4$ inclusions are 55 ~70 cm^3/mol (Fig. 6). The CO_2–$H_2O \pm CH_4$ inclusions may reflect a carbonic fluid, such as that within the early quartz, which was subsequently modified by fluid/rock reaction with surrounding rocks.

Variable X_{CO2} values are especially common for the CO_2–$H_2O \pm CH_4$ inclusions (Figs. 6, 7). This can be caused by several factors, such as immiscibility, fluid-wallrock interaction, progressive evolution of exsolved magmatic fluid, or inclusion necking-down (e.g., Ramboz et al. 1982; Olsen 1987; Lattanzi et al. 1989; Nwe

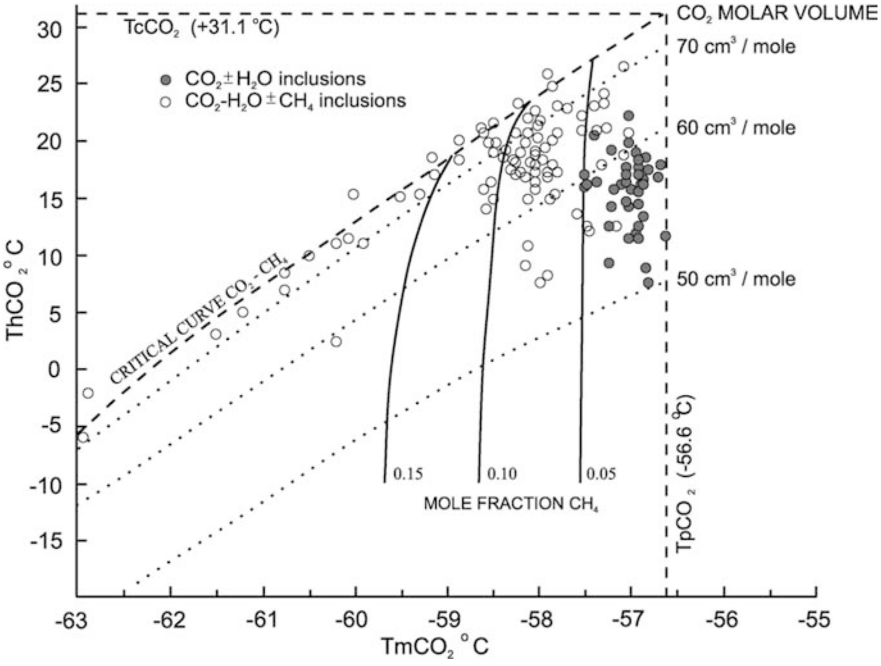

Fig. 6 Homogenization ($ThCO_2$) vs. melting temperature ($TmCO_2$) of CO_2–H_2O and CO_2-$H_2O \pm CH_4$ fluid inclusions. In the figure, the relations are shown between (1) molar fractions CH_4 (X_{CH4} = 0.05–0.15), (2) molar volumes (50–70 cm^3/mol) and various combinations of homogenization temperatures and melting temperatures for fluid inclusions in the CO_2–CH_4 system (data from van den Kerkhof et al. 1990; Thiéry et al. 1994). *Tp* CO_2 triple point of pure CO_2; *Tc* CO_2 critical temperature of pure CO_2

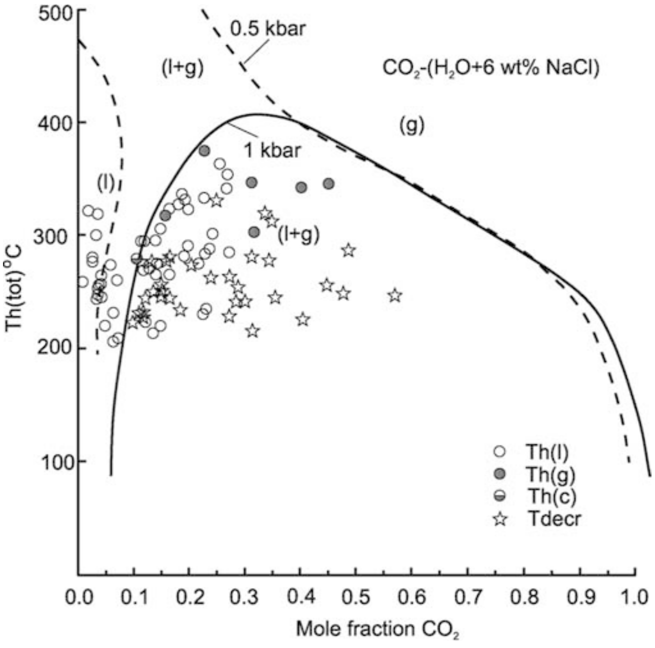

Fig. 7 Total homogenization temperature (Thtot) versus calculated equivalent mole fraction CO_2 of CO_2-$H_2O \pm CH_4$ inclusions. The curves delimit the two-phase regions in the H_2O–6 wt% NaCl system at 0.5 and 1 kbar. *l* liquid; *g* gas; *c* critical; *decr* decrepitation. Data after Bowers and Helgeson (1983)

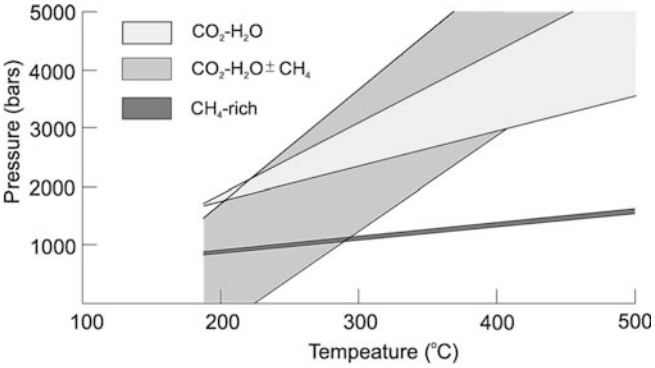

Fig. 8 Isochore plots for fluid inclusions from the Sanshandao deposit assuming a H_2O–CO_2–NaCl–CH_4 system. *Dotted region* presents P–T estimates for trapping conditions of CO_2–H_2O inclusions, *light gray region* and *light gray shaded regions* are calculated from CO_2–$H_2O \pm CH_4$ inclusions and CH_4-rich inclusions, respectively

and Grundmann 1990; Craw et al. 1993; Nabelek and Ternes 1997). Heterogeneous trapping of immiscible fluids would result in various phase ratios and two different modes of final homogenization (L, V) (Ramboz et al. 1982). Such variability was only observed from the CO_2–$H_2O \pm CH_4$ inclusions in some of the studied sections. If immiscibility did occur at Sanshandao, then it was only of local importance.

Some CH_4-rich inclusions are distributed along the critical curve of CO_2-CH_4 (Fig. 6). This implies initial fluids were more CO_2-rich, and then CH_4 was introduced into the gold-transporting fluids. Some authors have suggested that fluid inclusions re-equilibrate by chemical diffusion processes of H_2 and H_2O (i.e., Hall and Bodnar 1990; Hall and Sterner 1995; Sterner et al. 1995; Ridley and Hagemann 1999). The CO_2–H_2O type fluid inclusions at Sanshandao contain mainly CO_2 and lesser CH_4 (Table 1 and Fig. 6). The possibility of fluid inclusion re-equilibration by diffusion of H_2 into the inclusions, according to reactions such as $CO_2 + 4H_2 = CH_4 + 2H_2O$, might explained the gold stage fluid inclusion composition.

Pressure-temperature estimation

Pressure-temperature estimation from fluid inclusions can be obtained by constructing isochores from microthermetric and fluid composition data (Shepherd et al. 1985; Brown and Hagemann 1995). Isochores were constructed for the CO_2–H_2O and CO_2–$H_2O \pm CH_4$ inclusions (Fig. 8), with the latter including the rare CH_4-rich inclusions, assuming a H_2O-CO_2-NaCl-CH_4 system (Jacobs and Kerrick 1981) and using MacFlincor software (Brown and Hagemann 1995). As pressure estimates are always difficult (Roedder and Bodnar 1980), the treatment of temperature and pressure here needs to be revised according to the following logic: Measured homogenization temperatures are X. Using these as minimum temperature values, a preliminary minimum pressure of P1 can be calculated from the isochores. Using this value of P1, trapping temperatures for the fluids can be estimated as X + Z. This revised trapping temperature can then be used to calculate a more accurate pressure of P2.

For pre-gold CO_2–H_2O fluid inclusions, the minimum homogenization temperature is 267 to 375 °C. The preliminary minimum pressure from Fig. 8 is about 2.1 kbar. The pressure correction at 2.1 kbar is about 170 °C (Roedder 1984). Thus, the trapping temperature for CO_2–H_2O fluid inclusions is from 437–545 °C. The recalculated trapping pressure from Fig. 8 is greater than 3 kbar.

Measured homogenization temperatures of CO_2–$H_2O \pm CH_4$ inclusions are 226–273 °C. These inclusions will have very low minimum pressure estimations from Fig. 8. Consequently, isochores constructed for CH_4-rich inclusions, the same generation as CO_2–$H_2O \pm CH_4$ inclusions, provide the best estimated preliminary minimum trapping pressure of 1 kbar. The pressure correction at 1 kbar is about 80 °C (Roedder 1984). Estimated trapping temperature for CO_2–$H_2O \pm CH_4$ inclusions is from 306–353 °C. The recalculated trapping pressure for CO_2–$H_2O \pm CH_4$ inclusions is 1.2–2 kbar.

Possible sources of ore-forming fluids and gold transport and deposition

The calculated oxygen isotope composition of the fluid varies between 7.0 and 10.9‰. The analyses of hydrogen isotopic composition, measured directly from inclusion fluid, gave a relatively narrow spread between −63.8 and −80.6‰. In the plot of δD vs. $\delta^{18}O$ (Fig. 5) eight quartz samples locate in or near the magmatic water box. This implies that a magmatic fluid may have been dominant at the Sanshandao deposit. Any regional metamorphic fluid component is regarded as minimal for the mineralization at the Sanshandao deposit, because the Mesozoic age of mineralization is about 2 billion years younger than the age of metamorphism in the basement rocks (Hu et al. 1998).

Gold is mostly transported in hydrothermal solutions as gold bisulfide [$Au(HS)^0$, $HAu(HS)_2^0$, $Au(HS)_2^-$] and gold chloride [$AuCl_2^-$, $AuCl^0$, $AuCl(OH)^-$] complexes (Hayashi and Ohmoto 1991; Seward 1991; Zotov et al. 1991; Gammons et al. 1994; Benning and Seward 1996). From the close association of gold with sulfides (pyrite and arsenopyrite), not only in the alteration zones but also in the stockwork quartz veins, combined with the nature of wallrock alteration and consideration of the aqueous geochemistry of gold, the most likely mechanism of gold transport in the Sanshandao deposit was as a reduced sulfur complex. The P–T conditions pertaining to formation of stockwork quartz veins, and concomitant alteration, obtained from fluid inclusion pressure estimation range from ≥3–1.2 kbar and 545–306 °C, thus supporting the $Au(HS)_2^-$ complex as the most likely gold bisulfide complex for gold transport.

Constraints on gold metallogeny

Estimated minimum (lithostatic ?) pressure for carbonic inclusions at Sanshandao is 1.2 to ≥3 kbar, corresponding to a depth of about 4–8 km. Fluid inclusion studies have shown that the deposit formed from CO_2-bearing fluids with generally minor concentrations of CH_4. At these depths, the high confining pressures would severely limit the distance fluids could penetrate into the host rocks. The disseminated styles of mineralisation in the deposit and the presence of CH_4 suggest that the fluids interacted either directly with the host rocks or with fluids in equilibrium with the host rocks. Thus, the fluids at Sanshandao contain more CH_4 compared to those reported for other "Jiaojia-type" or "Linglong-type" gold deposits in the Zhaoyuan-Laizhou gold belt (Lu et al. 1999; Shen et al. 2000).

When the Sanshandao gold deposit is compared with other orogenic gold deposits (Table 3), a close resemblance is noted, especially with regard to the type of deposits, mineralogy, lithologies, structural settings, alteration patterns, character of the ore fluids and the inferred tectonic environment. Goldfarb et al. (2001) included the Jiaodong peninsula, where the Sanshandao gold deposits are located, as an example of district with significant orogenic gold lodes. We interpret that these orogenic gold deposits formed during exhumation of the basement subsequent to the collision of the North and South China cratons. Alternatively, these deposits may have formed during the early stages of subduction of the Pacific oceanic plate beneath China (Lu and Kong 1993; Wei and Qiu 1993; Yang and Lu 1996; Zhai and Deng 1996; Qiu et al. 2002).

The major gold mineralization in the Jiaodong province is hosted in Mesozoic granitoids, in contrast to other Precambrian cratons, where major gold deposits are hosted in Archaean greenstone belts (e.g., the Yilgarn in Western Australia and the Superior Province of Canada). The Sanshandao and other deposits of the Jiaodong gold province are mostly structurally con-

Table 3 A comparison between orogenic gold systems (Goldfarb et al. 2001; Groves et al. 1998; Kerrich and Cassidy 1994) and the intrusive-hosted Sanshandao gold deposit (this study)

Features	Orogenic gold system	Sanshandao
Regional scale:		
Setting	Structure traps, near large-scale (often transcrustal) faults	Localization controlled by first-order regional fault
Host rocks	Variable, deformed metamorphic terranes of all ages	Granodiorite intrusion
Spatial relations to intrusives	Common	Yes
Depth of formation	3–10 km	ca. 4–8 km
Tectonic environment	Commpressive	Commpressive ?
Timing of Au introduction:		
Age/date	Syn-metamorphic, syn-orogenic	After plutonic, syn-orogenic ?
Common Pb-isotopes	Old source involved	Primitive signature (Yang et al. 1998)
Ore features:		
Alterations	Carbonation, sulfidation, alkali metasomatism	Sericitization, sulfidation, K-feldspar, chloritization
Gold paragenesis	Sulfide and carbonate minerals, albite, scheelite, tourmaline	Sulfide and carbonate minerals
Depositional mechanism	Changing pH, T and element activities	P drop, mineral reaction
Ore solution characteristics:		
Fluid inclusions	H_2O–$CO_2 \pm CH_4$ fluid, low-salinity, near-neutral pH, reducing, $CO_2 \geq 5$ mol%, 200 to 400 °C	CO_2–$H_2O \pm CH_4$ fluid, low salinity reducing, 306 to 353 °C (CO_2–$H_2O \pm CH_4$inclusion)
Stable isotopes	$\delta^{18}O = +5$ to $+10$‰ $\delta D = +10$ to -60‰	$\delta^{18}O = +7.0$ to 10.9‰ $\delta D = -63.8$ to -80.6‰

trolled. They occur in faults and shear zones that cut the Mesozoic granitoids. Because the ore-controlling structures cut the Mesozoic granitoids, the deposits cannot be related to those larger Mesozoic, 160–156 Ma and 130–126 Ma, granitic plutons (Wang et al. 1998; Qiu et al. 2002; Zhai et al. 2002). Recently, Yang (2000) and Yang and Zhou (2000), using the Rb-Sr method on pyrite in gold-bearing quartz veins, directly dated the age of formation of the Linglong gold deposit (Linglong-style) in the north-western Jiaodong province as 121.6–122.7 Ma. Zhang et al. (2003) also reported a well-defined ^{40}Ar-^{39}Ar age of sericite at Cangshang gold deposit (Jiaojia-style) of 121.3 ± 0.2 Ma. Thus both styles of mineralization in Jiaodong gold province are coeval. In addition, the ages of the host rocks and a post-mineralization feldspar porphyry dyke in the Linglong goldfield, determined by the SHRIMP zircon U-Pb technique, constrained the age of gold mineralization as between 126 and 120 Ma (Wang et al. 1998; Qiu et al. 2002). Yang (2000) determined the ages of three mafic to intermediate dykes as 122–124 Ma (K-Ar method), similar to the age of the gold mineralization. The close temporal relation between the gold deposits and the 120–126 Ma mafic dikes may indicate that the magmatic water was derived from the degassing of mafic magmas parental to the dikes. Therefore, it is concluded that the ore fluids responsible for mineralization at the Sanshandao gold deposit were derived from fluids degassed from mafic to intermediate magmas.

Conclusions

Auriferous granitoid-hosted disseminated and vein/veinlet stockwork mineralization is common throughout Jiaodong gold province. Gold deposits occur typically along first-order regional faults, which are surrounded by broad alteration halos. Fluid inclusion studies of the stockwork system from the Sanshandao deposit indicate a range of fluid compositions with ubiquitous low salinity, CO_2-rich fluids. Methane was present in the fluids trapped during the mineralizing stages. Aqueous fluid inclusions, with lower salinity, represent the latest fluid composition in the hydrothermal system. Stable isotope data suggest that most of the ore fluid was of magmatic origin. A variety of fluid processes have been responsible for gold precipitation including fluid-wall-rock interactions and fluid immiscibility. Additionally, chemisorption processes in the interface between the fluid and the precipitating pyrite and arsenopyrite may have further enhanced the deposition of the gold, particularly on the surfaces of these sulfide minerals.

Acknowledgements Financial support was provided by the Key Program of Chinese Academy of Sciences (No. KZCX1-07) and the State Key Basic Research Development Program of China (No. G1999043207). Special thanks are due to the managements and staff of the Sanshandao Mine for their hospitality during the fieldwork. Dr. Yumin Qiu is thanked for constructive comments that helped the improvement of the paper. Mineralium Deposita editors Richard Goldfarb and Larry Meinert are thanked for helpful reviews and improving our English.

References

Bakker RJ (1997) Clathrates: Computer programs to calculate fluid inclusion V-X properties using clathrate melting temperatures. Comput Geosci 23:1–18

Benning LG, Seward TM (1996) Hydrosulphide complexing of gold (I) in hydrothermal solutions from 150 to 500 °C and 500 to 1500 bars. Geochim Cosmochim Acta 60:1849–1871

Bodnar RJ (1993) Revised equation and stable for determining the freezing point depression of H_2O-NaCl solutions. Geochim Cosmochim Acta 57:683–684

Bowers TS, Helgeson HC (1983) Calculation of the thermodynamic and geochemical consequences of nonideal mixing in the system H_2O–CO_2–NaCl on phase relations in geologic systems: equation of state for H_2O–CO_2–NaCl fluids at high pressures and temperatures. Geochim Cosmochim Acta 47:1247–1275

Brown PE, Hagemann SG (1995) MacFlincor and its application to fluids in Archaean lode-gold deposits. Geochim Cosmochim Acta 59:3943–3952

Burke EA (2001) Raman microspectrometry of fluid inclusions. Lithos 55:139–158

Burruss RC (1981) Analysis of phase equilibria in C-O-H-S fluid inclusion, in: Hollister LS, Crawford ML (eds) Short course handbook. Mineralogical Association of Canada 6, pp 39–74

Chen GY, Shao W, Sun DS (1989) Genetic mineralogy of gold deposits in Jiaodong region with emphasis on gold prospecting (in Chinese with English abstract). Chongqing Publishing House, Chongqing, pp 181–224

Clayton RN, Mayeda TK (1963) The use of bromine pentafluoride in the extraction of oxygen from oxides and silicates for isotopic analysis. Geochim Cosmochim Acta 27:43–52

Clayton RN, O'Neil JR, Mayeda TK (1972) Oxygen isotope exchange between quartz and water. J Geophys Res B77:3057–3067

Craw D, Teagle DAH, Belocky R (1993) Fluid immiscibility in late-Alpine gold-bearing veins, eastern and northwestern European Alps. Miner Deposita 28:28–36

Diamond LW (1992) Stability of CO_2 clathrate + CO_2 vapor + aqueous KCl-NaCl solutions: experimental determination and application to salinity estimates of fluid inclusions. Geochim Cosmochim Acta 56:273–280

Diamond LW (2001) Review of the systematics of CO_2–H_2O fluid inclusions. Lithos 55:69–99

Frieman I (1953) Deuterium content of natural water and other substances. Geochim Cosmochim Acta 4:89–103

Gammons CH, Williams-Jones AE, Yu Y (1994) New data on the stability of gold (I) chloride complexes at 300 °C. Mineral Mag 58A:309–310

Goldfarb RJ, Groves DI, Gardoll S (2001) Orogenic gold and geologic time: a globe synthesis. Ore Geol Rev 18:1–75

Groves DI, Goldfarb RJ, Gebre-Mariam M, Hagemann SG, Robert F (1998) Orogenic gold deposit: a proposed classification in the context of their crustal distribution and relationship to other gold deposit type. Ore Geol Rev 13:7–27

Hall DL, Bodnar RJ (1990) Methane in fluid inclusions from granulites: a product of hydrogen diffusion. Geochim Cosmochim Acta 54:641–651

Hall DL, Sterner SM (1995) Experimental diffusion of hydrogen into synthetic fluid inclusions in quartz. J Metamorph Geol 13:345–355

Hayashi KI, Ohmoto H (1991) Solubility of gold in NaCl- and H_2S-bearing aqueous solutions at 250–350 °C. Geochim Cosmochim Acta 55:2111–2126

Hollister LS, Burruss RC (1976) Phase equilibria in fluid inclusions from the Khtada metamorphic complex. Geochim Cosmochim Acta 40:163–175

Hu SX, Wang HN, Wang DZ, Zhang JR (1998) Geology and geochemistry of gold deposits in east China (in Chinese with English abstract). Science Press, Beijing, pp 77–86

Jacobs GK, Kerrick DM (1981) Methane: an equation of state with application to the ternary system H_2O–CO_2–CH_4. Geochim Cosmochim Acta 45:607–614

Kerrich R, Cassidy KF (1994) Temporal relationships of lode gold mineralization to accretion, magmatism, metamorphism and deformation, Archaean to present: a review. Ore Geol Rev 9:263–310

Lattanzi PR, Curti E, Bastogi M (1989) Fluid inclusion studies on the gold deposits of the Upper Anzasca valley, northwestern Alps, Italy. Econ Geol 84:1382–1397

Lu G, Kong Q (1993) Geology of the Linglong-Jiaojia type gold deposits (in Chinese with English abstract). Scientific Publishing House, Beijing, 253 pp

Lu HZ, Guha J, Fang GB (1999) Characteristics of ore-forming fluid in Linglong gold mine, Shandong, China (in Chinese with English abstract). Geochimica 28:421–437

Matsuhisa Y, Goldsmith JR, Clayton RN (1979) Oxygen isotopic fractionation in the system quartz-albite-anothite-water. Geochim Cosmochim Acta 43:1131–1140

Nabelek PI, Ternes K (1997) Fluid inclusions in the Harney Peak Granite, Black Hills, South Dakota, USA: implications for solubility and evolution of magmatic volatiles and crystallization of leucogranite magmas. Geochim Cosmochim Acta 61:1447–1465

Nwe YY, Grundmann G (1990) Evolution of metamorphic fluids in shear zones: the record from the emeralds of Habachtal, Tauern Window, Austria. Lithos 25:281–304

Olsen SN (1987) The composition and role of the fluid in migmatites: a fluid inclusion study of the Front Range rocks. Contrib Mineral Petrol 96:104–120

Qiu YM, Groves DI, McNaughton NJ, Wang LG, Zhou TH (2002) Nature, age, and tectonic setting of granitoid-hosted, orogenic gold deposits of the Jiaodong Peninsula, eastern North China craton, China. Miner Deposita 37:283–305

Qiu YS (1989) Regional geological setting of gold deposits in the Zhaoye Gold Belt in Shandong Province (in Chinese). Liaoning Science and Technology Press, Shenyang, pp 1–153

Ramboz C, Pichavant M, Weisbrod A (1982) Fluid immiscibility in natural processes: Use and misuse of fluid inclusion data. II. Interpretation of fluid inclusion data in terms of immiscibility. Chem Geol 37:29–46

Ridley JR, Hagemann SG (1999) Interpretation of post-entrapment fluid-inclusion re-equilibration at the Three Mile Hill, Marvel Loch and Griffins Find high-temperature lode-gold deposits, Yilgarn Craton, Western Australia. Chem Geol 154:257–278

Roedder E (1984) Fluid inclusions. Rev Mineral 12:644 pp

Roedder E, Bodnar RJ (1980) Geological pressure determinations from fluid inclusion studies. Annu Rev Earth Planet Sci 8:263–301

Seward TM (1991) The hydrothermal geochemistry of gold. In: Foster (ed) Gold metallogeny and exploration. Blackie, London, pp 37–62

Shen K, Hu SX, Sun JG, Ling HF, Zhao YY, Sun MZ (2000) Characteristics of ore-forming fluids of the Dayinggezhuang gold deposit in Jiaodong, China (in Chinese with English abstract). Acta Petrol Sin 16:542–550

Shepherd TJ, Rankin AH, Alderton DHM (1985) A practical guide to fluid inclusion studies. Blackie, London, 239 pp

Sterner SM, Hall DL, Keppler H (1995) Compositional re-equilibration of fluid inclusions in quartz. Contrib Mineral Petrol 119:1–15

Taylor HP (1979) Oxygen and hydrogen isotope relations in hydrothermal ore deposits. In: Barnes (ed) Geochemistry of hydrothermal ore deposits. Wiley, New York, pp 236–277

Thiéry R, van der Kerkhof AM, Dubessy F (1994) VX properties of CH_4-CO_2 and CO_2-N_2 fluid inclusions: modeling for $T < 31$ °C and $P < 400$ bar. Eur J Mineral 6:753–771

van den Kerkhof A (1990) Isochoric phase diagram in the system CO_2-CH_4 and CO_2-N_2: application to fluid inclusions. Geochim Cosmochim Acta 54:621–629

van den Kerkhof A (2001) Carbonic inclusions. Lithos 55:49–68

van den Kerkhof A, Thiéry R (1994) Phase transitions and density calculation in the CH_4-CO_2-N_2 system. In: De Vivo B, Frezzotti ML (eds) Fluid inclusions in minerals, methods and application. Short course handbook of the IMA working group, Pontignano-Siena, pp 171–190

Wang LG, Qiu YM, McNaughton NJ, Groves DI, Luo ZK, Huang JZ, Miao LC, Liu YK (1998) Constraints on crustal evolution and gold metallogeny in the northeastern Jiaodong Peninsula, China, from SHRIMP U-Pb zircon studies of granitoids. Ore Geol Revs 13:275–291

Wei YE, Qiu YS (1993) Research on gold deposit geology of Eastern China. Geological Memoirs Series 4:107–116 (in Chinese with English abstract)

Xu JH, He ZL, Xie YL (1996) Geochemistry of ore-forming fluids of gold deposits in greenstone belt (in Chinese with English abstract). Geological Publishing House, Beijing, 99 pp

Yang JH (2000) Age and metallogenic dynamics of gold mineralization in Jiaodong Peninsula, eastern China: constraints on the interaction of mantle/crust and metallogenesis/lithospheric evolution (in Chinese with English abstract). PhD Thesis, Institute of Geology and Geophysics, Chinese Academy of Sciences, Beijing, 133 pp

Yang JH, Zhou XH (2000) The Rb-Sr isochron of ore and pyrite sub-samples from Linglong gold deposit, Jiaodong Peninsula, eastern China and their geological significance. Chin Sci Bull 45:2272–2276

Yang JH, Zhou XH (2001) Rb-Sr, Sm–Nd, and Pb isotope systematics of pyrite: Implications for the age and genesis of lode gold deposits. Geology 29:711–714

Yang MZ, Lu GX (1996) The geology-geochemistry of gold deposits of the greenstone belt in Jiaodong district (in Chinese with English abstract). Geological Publishing House, Beijing, 228 pp

Yang ZF, Xu JK, Zhao LS, Shen YL, Wu YB (1998) The evolution of regional crust and the geochemistry on gold mineralization in Jiaodong (in Chinese with English abstract). Geological Publishing House, Beijing, pp 112–122

Zhai MG, Yang JH, Fan HR, Miao LC, Li YG (2002) A large-scale cluster of gold deposits and metallogenesis in the eastern China craton. Int Geol Rev 44:458–476

Zhai MG, Yang JH, Liu WJ (2001) Large clusters of gold deposits and large-scale metallogenesis in the Jiaodong Peninsula, eastern China. Sci China (Ser D): 44:758–768

Zhai Y, Deng J (1996) Outline of the mineral resources of China and their tectonic setting. Aust J Earth Sci 43:673–685

Zhang XO, Cawood PA, Wilde SA, Liu RQ, Song HL, Li W, Snee LW (2003) Geology and timing of mineralization at the Cangshang gold deposit, north-western Jiaodong Peninsula, China. Miner Deposita 38:141–153

Zhou TH, Lu GX (2000) Tectonics, granitoids and Mesozoic gold deposits in east Shandong, China. Ore Geol Rev 16:71–90

Zotov A, Baranova N, Dar'yina T, Bannykh L (1991) The solubility of gold in aqueous chloride fluids at 350–500 °C and 500–1500 atm. Thermodynamic parameters of $AuCl_2^-$(sol) up to 750 °C and 500 atm. Geochem Int 28:63–71